ARTICLE

JOURNAL`S UNIVERSITY OF BABYLON FOR ENGINEERING SCIENCES (JUBES)

مـــجلـة جـــامعة بـــابـل للعلـــوم الهندسية

Vol. 32, No. 3. \ 2024 ISSN: 2616 - 9916

Comparison Among Three Adsorbent Materials Al_2O_3/ Aloe vera Gum Nanocomposites, Al_2O_3 Nanoparticles, and Fly Ash to Phosphate Removal from Tigris River

Ghalib J. k. Al-Sumaidaie[a] **Muzher M. I. AL-Doury**[b]

[a]*Department of Chemical Engineering, College of Engineering, Tikrit University, Tikrit, Iraq*

Email: Kalab.j.kadem44336@st.tu.edu.iq, ORCID: https://orcid.org/0009-0006-5429-8852

[b]*Petroleum and Gas Refining Engineering Department, Petroleum Processes Engineering College, Tikrit University, Tikrit, Iraq*

Email: samuzhermahdi@tu.edu.iq ; ORCID: https:// orcid.org/0000-0002-5149-945X

Received: 28/1/2024 **Accepted:** 18/3/2024 **Published:** 27/6/2024

Abstract

Modern, promising and environmentally friendly nanomaterials was used as adsorbent material, [AL_2O_3 Nanoparticles, loaded Aloe vera Gum]. It is a natural material that is secreted from the (Aloe vera plant) based nanocomposites using sol-gel method to increase the surface area to Phosphate removal.

Selectors within a range are dose of (Al_2O_3/AG) nanoparticles (20-100 mg), initial ion concentration (Ci) 3.7-10.7 mg/L. pH for solution 3,4,5,7, and 9, contact time 5-100 minutes, wavelength of light (yellow, white, red, green, blue, and sunlight), and magnetic field (MF) 300-500 mTesla. Batch experiments were conducted using The Hanna Phosphate High-Range Checker.

Results showed the best dose 60 mg, pH 5, wavelength red, contact time 100 min and C_i of PO_4^{-3} at 7.6 mg/L. It is found that the Langmuir adsorption model fairly fits the experimental data; while the pseudo-second-order kinetic model fits the adsorption. The adsorption capacity is increased with the decrease of initial concentration of the pollutant (phosphate) and is directly proportional to the dose of Al_2O_3/AG nanocomposites adsorbent.

The best conditions obtained using Al_2O_3/AG is compared with fly ash and Al_2O_3 NPs. The surface area of Al_2O_3/AG nanocomposites was recorded as 124.255 m^2. g^{-1}. The best operating condition that gives the highest removal was used to test AL_2O_3 NPs and fly ash**.** It is proved that AL_2O_3/AG gives higher removal than that of AL_2O_3 NPs and fly ash.

Keywords: Adsorption capacity, Aloe vera Gum (AG), Al_2O_3 Nanoparticles, Light intensity, Phosphate, Removal efficiency.

1. Introduction

Phosphate poisoning can occur in both humans and animals and manifests primarily as gastrointestinal distress. The effects of phosphorus on plants and the aging of marine life in its vicinity are the most crucial aspects of this element in surface water[1 and [2]. Eutrophication can happen when there is more phosphate in an aquatic environment as shown in **Figure 1**. This process speeds up the natural aging process in that environment. Because of eutrophication, there are more plankton and algae, which throws off the normal cycle of making things and eating them. At first, this will increase the number of water animals because there will be more food [3]

Figure 1 Water Poisoning as a Result of Phosphorous Pollution Causes Increased levels of Nutrients. It can lead to Water Pollution and Algae Blooms

To remove phosphate from water and water bodies, there are many methods, the most important of which is the adsorption method, which is one of the common methods that do not need complex conditions [4]. The selection of diverse adsorbents for the adsorption of phosphate was implemented, yielding favorable outcomes. However, the method was deemed unsuitable for extensive implementation. Consequently, the development of a carbon-based nanocomposite sorbent that is both cost-effective and readily available, while also exhibiting high efficacy, is imperative for efficient removal of pollutants and anionic nutrients [5], the carbon-based nanocomposite exhibits distinct benefits compared to alternative adsorbents due to its notable efficacy, lack of harmful properties, economical value, and potential for widespread implementation. [6]. Biological removal processes; such as used activated sludge and used algae-based treatment [7and 8].

Advanced removal processes; such as metal-organic frameworks (MOFs) adsorption, adsorption by zirconium and its composites and adsorption by nanostructured binary oxides**.** The selection of diverse adsorbents for the adsorption of phosphate was implemented, yielding favorable outcomes. However, the method was deemed unsuitable for extensive implementation. Consequently, the development of a carbon-based nanocomposite sorbent that is both cost-effective and readily available, while also exhibiting high efficacy, is imperative for efficient removal of pollutants and anionic nutrients [5].

The method adsorption by nanostructured binary oxides was chosen for the purpose of this study. It was used alumina nanoparticles on porous activated carbon as a support material for catalyst as adsorbent material to phosphate removal.

There are many studies that depend on alumina nanoparticles loaded either on gum or other catalyst.

Below Table 1 shows some studies and the findings of the researchers

Table 1 Comparison of Catalytic Activity of Al_2O_3/AG Nanocomposites with Similar Kinds of Studies

Catalyst with NPs	Removal Efficiency, %	Adsorbent Dose (mg)	Contact Time, min.	Surface Area ($m^2.g^{-1}$)	Reference
Guar gum/Al_2O_3	90	100 mg	220	154.22	[9]
Al_2O_3/Fe_2O_3	75	200 mg	90	97.45	[10]
Al_2O_3/MOG	95	10 mg	75	176.92	[11]
Ag–AgO/Al_2O_3	81	15 mg	90	105.47	[12]
Al_2O_3/Morina gum	84	45 mg	105	111.85	[13]
Al_2O_3/AG	86	60 mg	100	124.255	Present study

The aim of this study is to remove phosphate compounds from Industrial water that contains different concentrations by adsorption technology using newly developed, promising and environmentally friendly adsorbents (alumina nanoparticles on aloe vera plant gum activated carbon (AG) as a support material for the catalyst as adsorbent material).

2. Description of the Study Area

Wastewater samples were taken from Tigris river near wastewater dumps in different regions of Salah Al-Din Governorate in (Sharqat, Baiji, Tikrit, Al-Alaam, Al-Dour, Samarra, Al-Dhuluiya, Balaad, and Dujail). Table 2 includes some characteristics of those samples while Figure 2 represents the location of sampling sites. Phosphates concentration found in some areas exceeds the permissible Iraqi specifications for the water disposed in the sewage pipes and dumped to the water source (the river) were the limit is (3 mg / liter). Below are the results of chemical analysis of water samples taken from approved sites within three months, which were conducted at the Salah al-Din Water Resources Laboratories.

Table 2 Some Properties of Water Samples Taken from Approved Sites During December 2022 – February 2023

Sec.	Location	Values For												coordinates UTM	
		pH			T.D.S			EC			PO_4 (ppm)			X	Y
		Dec.	Jan.	Feb.	Dec.	Jan.	Feb.	Dec.	Jan.	Feb.	Dec.	Jan.	Feb.		
1	Sharqat district	8.22	7.48	7.89	239	245	242	478	488	469	0.8	1.2	1.1	340541	3933205
2	Baiji district	8.32	8.15	8.12	243	233	263	485	458	475	1.2	1.5	4.6	367363	3855400
3	Al alaam district	7.90	7.47	7.88	233	231	238	467	467	467	1.8	1.3	2.3	377847	3844058
4	Al alaam irrigation channel	8.01	8.15	8.12	235	235	239	469	489	479	2.1	2.8	2.2	377922	3843969
5	Tikrit district	8.18	8.03	8.03	233	245	243	466	496	466	1.1	1.8	1.4	378172	3837034
6	Al-Dour district	8.40	8.18	8.23	229	239	249	459	489	451	4.3	2.3	2.7	388150	3813850
7	Samarra district	8.35	8.69	8.34	261	261	231	522	514	532	2.8	2.1	2.8	395314	3782421
8	Rasasi in Samarra	8.46	8.42	8.46	277	276	279	555	571	561	2.1	2.2	2.1	394022	3794572
9	Dhuluiya district	8.08	8.12	8.09	340	340	341	680	691	583	2.8	1.8	2.8	435711	3770620
10	Rasasi,in Dhuluiya	8.07	8.07	8.12	301	305	341	602	652	623	5.5	4.5	2.5	423870	3774225
11	AL-Azim in Dhuluiya	8.09	8.22	8.71	2040	2015	2079	4070	4145	4056	4.6	3.6	2.6	438577	3773404
12	Balaad district	8.45	7.98	8.23	2281	2191	2212	4563	4458	4769	3.4	2.8	2.4	425872	3765486
13	Dujail district	7.98	7.78	7.89	2128	2178	2110	4256	4358	4212	3.2	3.3	3.3	444057	3742478

ARTICLE
JOURNAL`S UNIVERSITY OF BABYLON FOR ENGINEERING SCIENCES (JUBES)
مـــجلـة جـــامعة بـــابـل للعلـــوم الهندسية
Vol. 32, No. 3. \ 2024 ISSN: 2616 - 9916

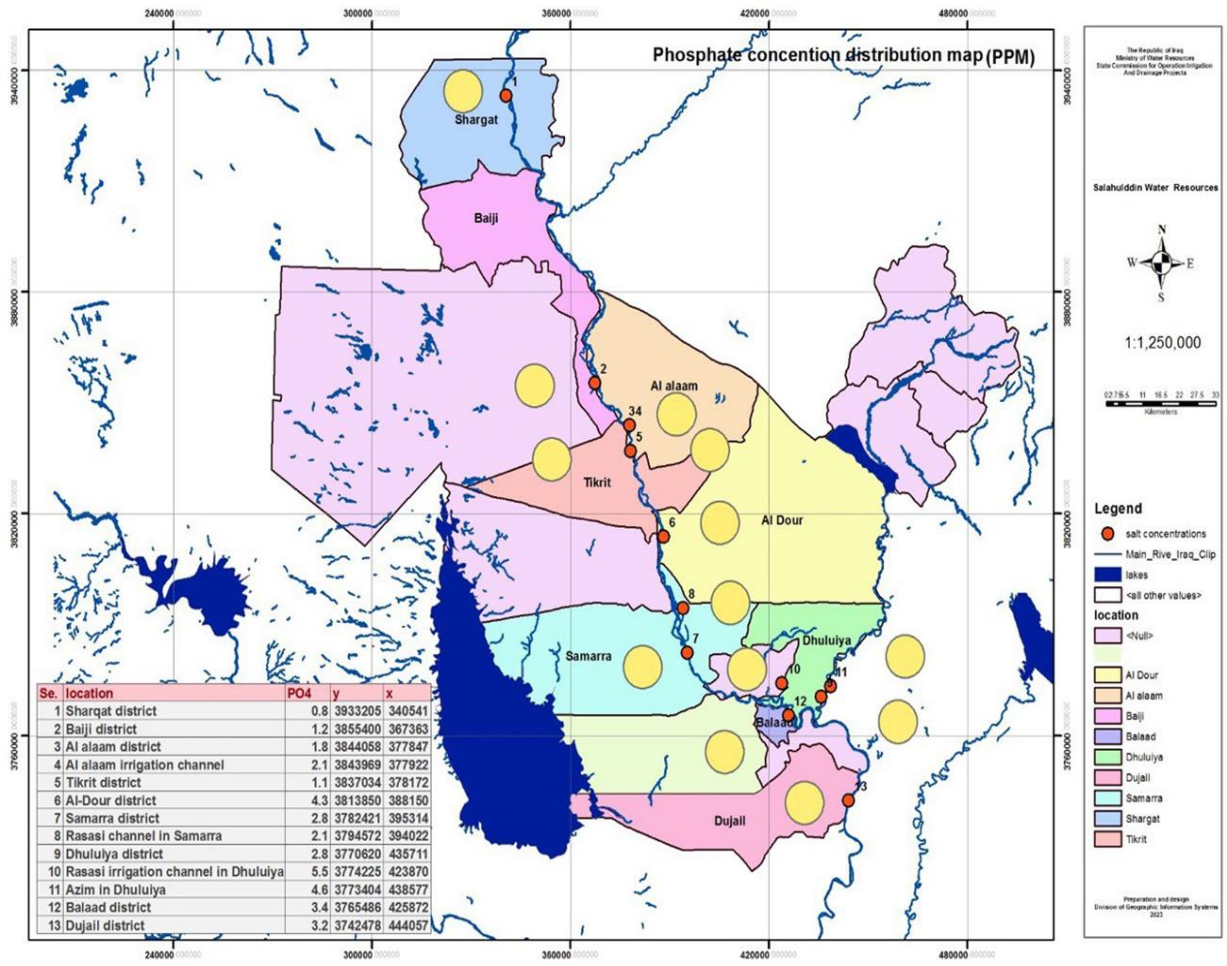

Se.	location	PO4	y	x
1	Sharqat district	0.8	3933205	340541
2	Baiji district	1.2	3855400	367363
3	Al alaam district	1.8	3844058	377847
4	Al alaam irrigation channel	2.1	3843969	377922
5	Tikrit district	1.1	3837034	378172
6	Al-Dour district	4.3	3813850	388150
7	Samarra district	2.8	3782421	395314
8	Rasasi channel in Samarra	2.1	3794572	394022
9	Dhuluiya district	2.8	3770620	435711
10	Rasasi irrigation channel in Dhuluiya	5.5	3774225	423870
11	Azim in Dhuluiya	4.6	3773404	438577
12	Balaad district	3.4	3765486	425872
13	Dujail district	3.2	3742478	444057

Figure 2 A Map with Coordinates Universal Transverse Mercator (UTM) Preparation and Design Division of Geographic Information Systems, Salah al-Din Water Resources, 2023

3. Experimental Program

3.1 Apparatus

ESP Ultraflat Magnetic Stirrer supplied by VELP Scientifica Srl, located in Italy, and has a speed of 1100 rpm. It is excellent for detecting particles and color shifts are used in current study. The Hanna Phosphate High-Range Checker®, the accuracy and resolution of chemical test kits are constrained due to their reliance on visual perception by the human eye for the detection of color variations and in order to accurately ascertain the concentration of ions, sophisticated instrumentation integrates a light source, such as an LED or tungsten lamp, with a filter and a light sensing detector. The Eco Testr pH Thermo Fisher Scientific Inc. Massachusetts, Waltham, USA. This device was relied on for the purpose of adjusting the acidic medium of the solutions used in this study.

3.2 Preparation Materials

3.2.1 Preparation of Aloe vera Gum (AG)

After collecting the gum for the aloe vera plant, drying it under sun rays, then washing with a concentrated acid solution at pH 3 of H2SO4 60% 3:1 (v/w), drying it again without nitrogen and isolated from air in the 110°C drying oven for 4 hours, then heating it to a temperature of 700 °C for 3 hours, and for the purpose of getting rid of acidity, it is washed with ion-free water for four consecutive times and then dried last so without nitrogen and isolated from air in the oven drying for 9 hours at 110°C.

3.2.2 Preparation of Al_2O_3/AG

Using the well-known Sol-gel method, Al2O3 nanoparticles It is a non-amorphous powder and homogenized made in the United States of America purchased from the local markets and has a particle size of 50 nm is loaded on activated carbon (AG) to form Al2O3/AG nanocomposites. Al2O3 is mixed with AG in a ratio of 2:1 (w/w) and then add a solution of sodium hydroxide (0.5 M) in a point with continuous mixing, the mixing period lasts for two hours for the purpose of homogenizing the solution, the solution is left for a period and then filtered for two times and washed between them with ethanol and deionized water, the result is dried in the drying oven for 6 hours and a temperature of 100 ° C. About which the powder Al2O3/AG nanocomposites is formed [11].

3.2.3 Preparation of Fly Ash

Fly ash is prepared by burning Reeds and Sedge that are found along river banks. Because of the possible grain composition of the fly ash, it was modified. NaOH solutions of 1M, 3M, and 6M were utilized for the modification. Fly ash was subjected to a 1:10 weight ratio treatment in NaOH solutions. After that, the mixture was incubated for 24 hours at 55° C. The mixture was filtered after treatment, carefully rinsed in distilled water, dried in an oven at 75° C. The finished solid products were then examined physically and chemically.

3.3 Adsorbent Characterization

The following section looks at how the created catalyst's surface area and pore volume are spread out (BET) techniques. And XRD, SEM were measured in each of the Alkhora company nano research lab in Baghdad. As well Oil Research and Development Center, Ministry of Oil.

3.3.1 The SEM images

SEM examines the surface morphologies of fly ash, Al2O3 NPs, and Al2O3/AG nanocomposites. The SEM images of fly ash are shown in Figure 3. From these images, the surface is relatively smooth, while for Al2O3/AG, shown in Figure 4 the surface becomes rough and micropores could be found obviously. pore volume values are a benefit for the adsorption of phosphate [13]. The SEM image for α-Al2O3 NPs shown in Figure 5 is very smooth clearly because it is completely homogeneous and equal in size to the nanoparticles due to its processing from US Research Nanomaterials.

The microscopic study shows that the surface of the fly ash is changing. It now has holes on its surface, which makes it look like a broken piece of ice. The Figure 3 shows that objects that look like hexagonal rods are being made.

Figure 4 shows SEM images that show the uneven spread of Al2O3NPs on the surface of AG, which looks like a hexagonal rod structure as shown in Figure 6.

The particles of AG tend to make a lot of macropores and mesopores, which were mostly filled with Al2O3 particles. This makes it easier for Al2O3 particles to absorb light and boosts their ability to act as photocatalysts [14]. When you look at Figures 5, you can see that pure Al2O3 NPs tends to group together into crystallites of equal sizes. Al2O3NPs also grow on the surface of AG, which makes the surface of Al2O3/AG nanocomposites rough and full of holes. Al2O3/AG nanocomposites had smaller particles than Al2O3NPs by themselves.[15] say that this type of small particle is a good choice for getting clear of both organic and artificial molecules.

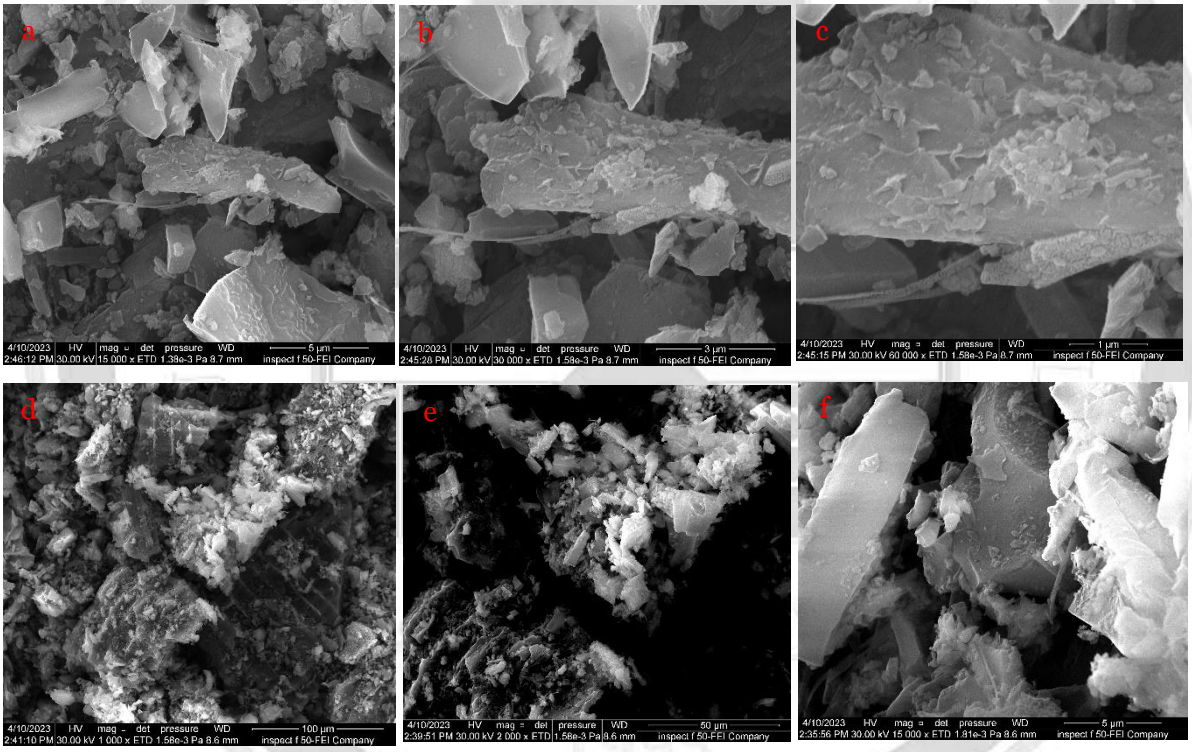

ARTICLE

JOURNAL`S UNIVERSITY OF BABYLON FOR ENGINEERING SCIENCES (JUBES)

مـــجلـة جـــامعة بـــابـل للعلـــوم الهندسية

Vol. 32, No. 3. \ 2024 ISSN: 2616 - 9916

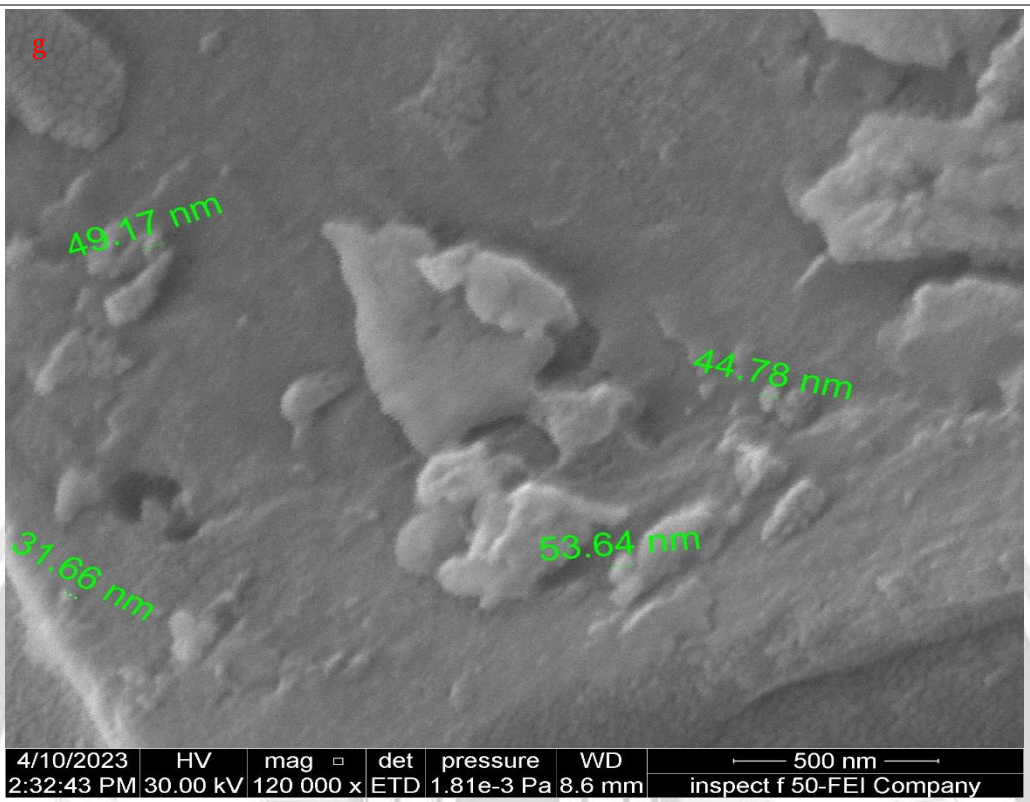

Figure 3 SEM Images for Fly Ash

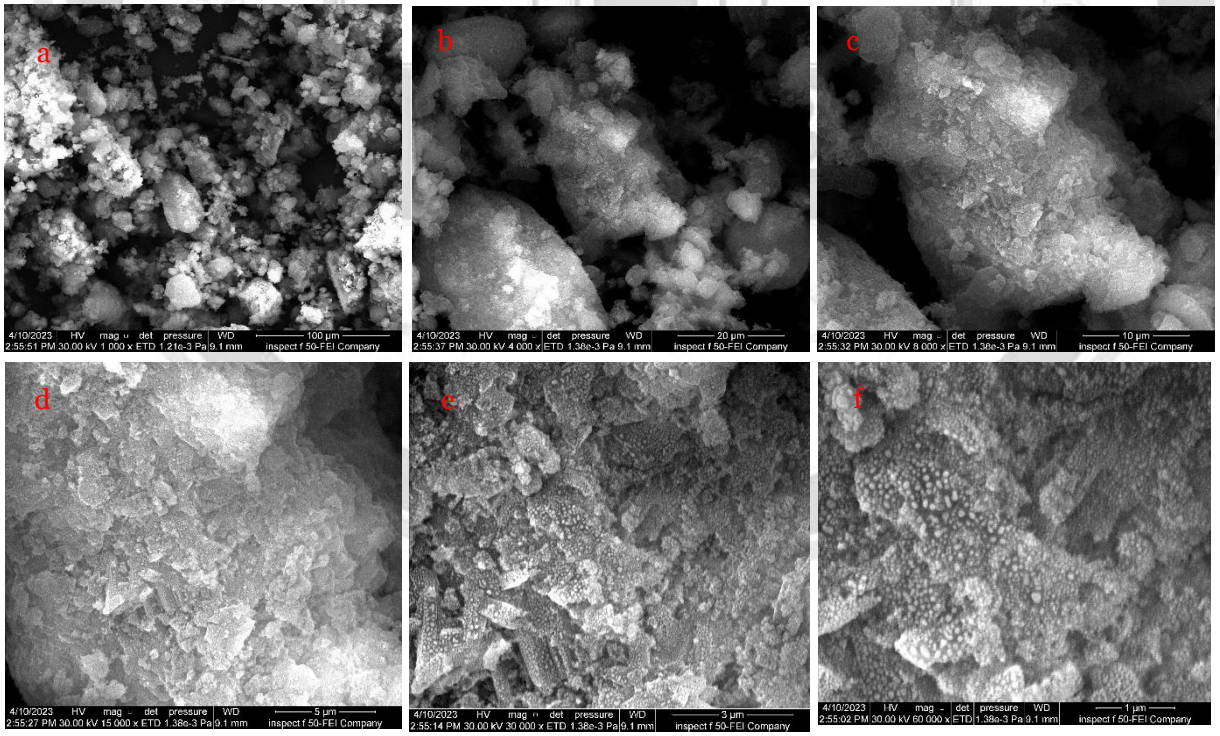

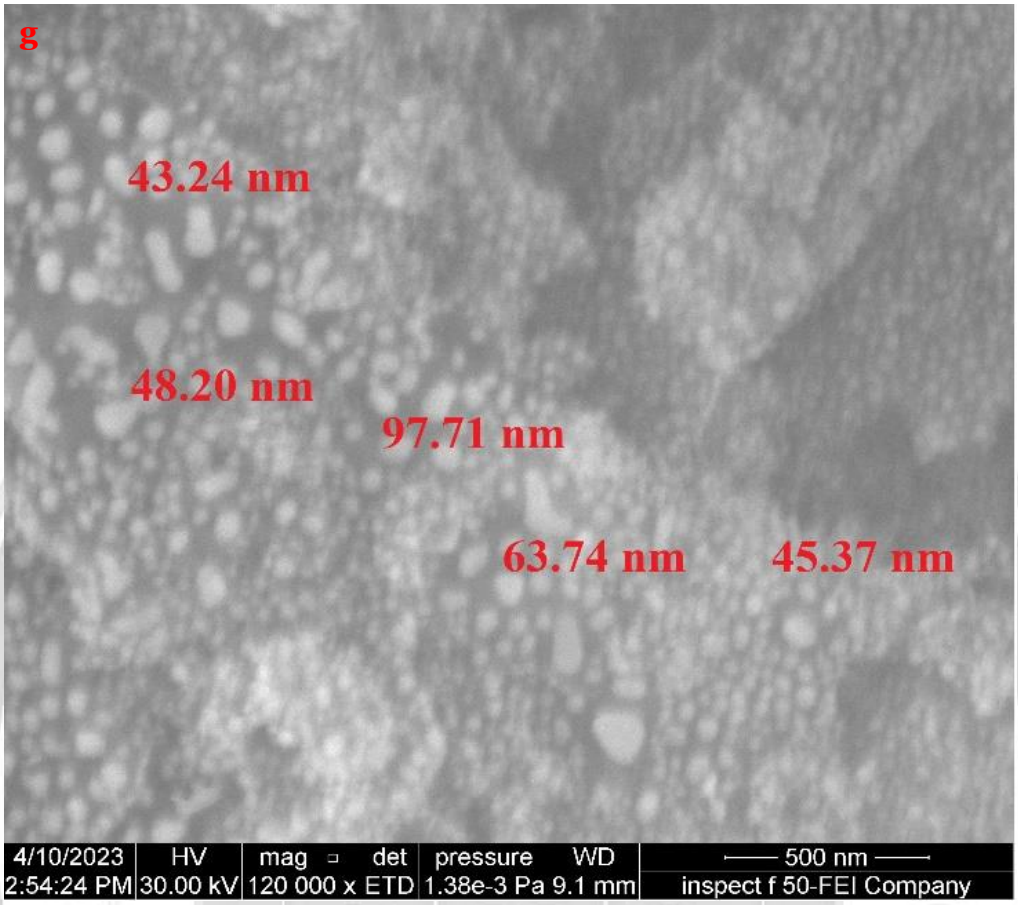

Figure 4 SEM Images for Al_2O_3/AG Nanocomposites

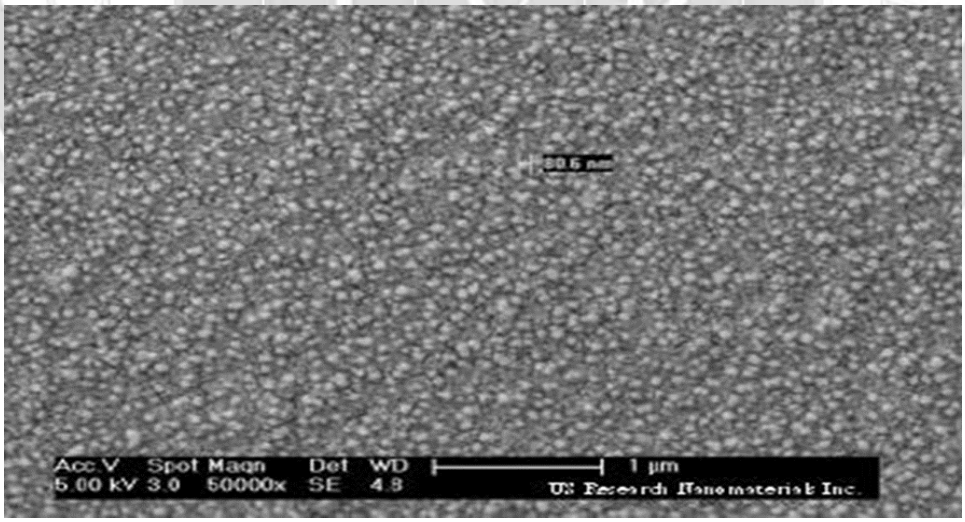

Figure 5 SEM Images for α-Al_2O_3 Nanoparticles the Sample Exhibits a Very Narrow Particle Size Range of 50 nm

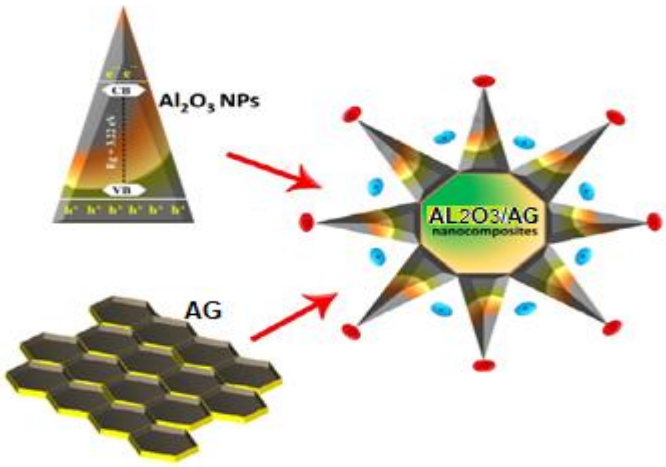

Figure 6 Predicted Shape of Both Molecule Al_2O_3 NPs, Fly Ash and Molecule Formation of Al_2O_3/AG Nanocomposites

3.3.2 The XRD analysis

Figure 7 shows the X-ray diffraction pattern of Al_2O_3/AG. It has a broad hump, which shows that the structure is primarily amorphous. The peaks are sharp and high, typical of Al_2O_3/AG indexed to the face of carbon.

The pattern for fly ash shows few peaks and rather small the diffraction peaks at 2θ values of 18.04°, 26.75°, 29.15°, 43.26°, and 47.9° **Figure 8**. Presence of no broad hump.

The pattern for AL_2O_3 NPs shown in **Figure 9** it also has peaks that match, but they are much weaker. They might act like a mask on AG, and their size has been cut down a lot, making the points less intense. When the average size of the crystallites gets smaller, the surface area of the AL_2O_3 particles supported by activated carbon gets bigger.

Figure 10 shows the X-ray diffraction (XRD) patterns of fly ash, Al_2O_3, and Al_2O_3/AG catalysts, for the purpose of easy comparison between different diffraction peaks.

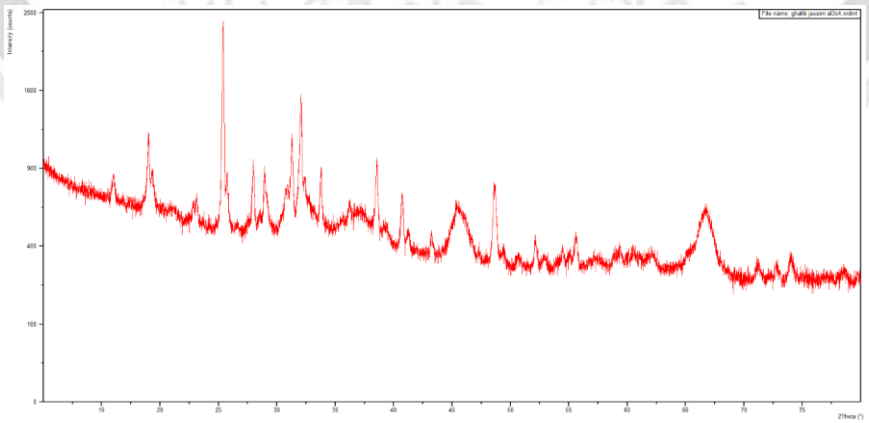

Figure.7 XRD Pattern of Al_2O_3/AG

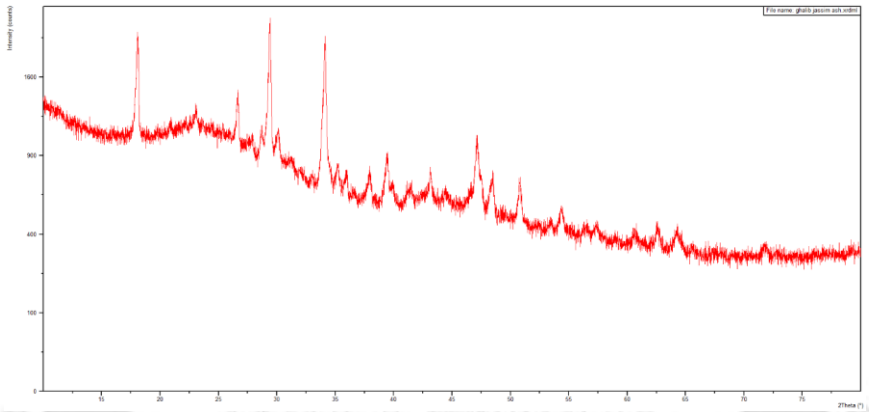

Figure 8 XRD Pattern of Fly Ash

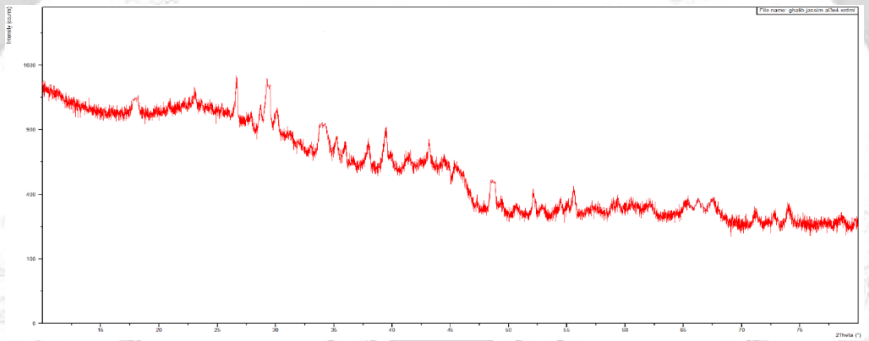

Figure 9 XRD Pattern of Al_2O_3 NPs

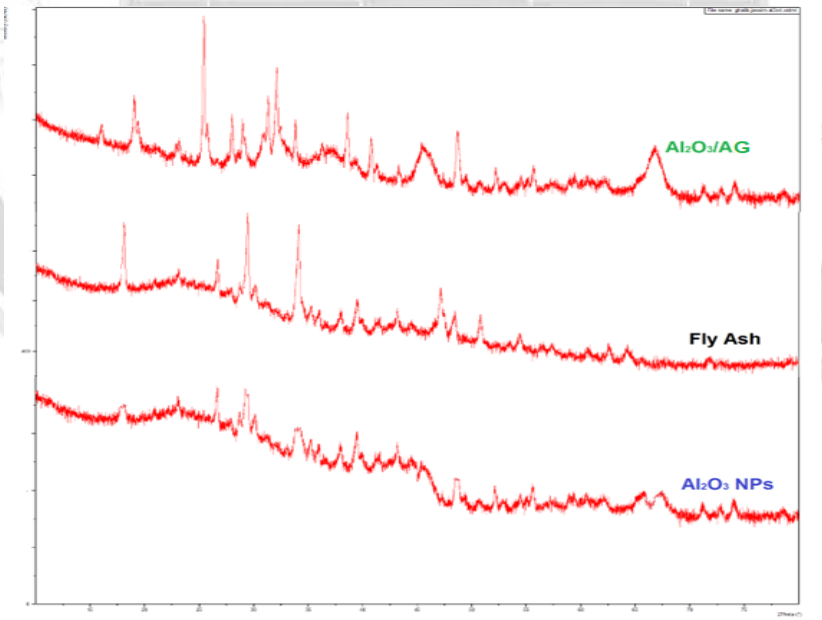

Figure 10 XRD Patterns of Al_2O_3 NPs Fly Ash and Al_2O_3/AG

3.3.3 The BET analysis

The analyzes of the surface area conducted on Ministry of Oil in Baghdad on the date 4/30/2023 as follows in **Table 3**

Table 3 BET Analyses

Sample name	Surface area, m^2/g	Method	Detection limit	Uncertainty value	Calibration (Internal or External)
Al_2O_3/AG	124.255	ISO 9277/2010	(0.1-2000)	0.182 %	Auto
Al_2O_3 NPs	51.235				
Fly ash	46.438				

The BET study of the nanocomposites shows what the surface looks like and how big the pores are. **Table 3** shows this. Also, a BET test was used to figure out that the surface area of Al_2O_3/AG nanocomposites is about 124.255 m^2/g. The ions can move through the sample with the right pore size and the right amount of surface area. This improves the binding efficiency and the photocatalytic potential of the sample. The Al_2O_3/AG nanocomposites made by chemical synthesis are very good at absorbing and breaking down light.

3.4 Experimental Procedure

The most critical elements influencing the processes are the initial concentration, the concentrations were taken through the Iraqi standard specifications allowed for the concentration of phosphate in the river, which was 3 mg/l up to 10 mg per liter, which is the highest expected measured value in the river. Dose of adsorbent Al2O3/AG nanocomposites, different dosage were taken to know the expected effect. Contact time,by conducting 24-hour test trials to find out the contact time. pH, basic, acidic and neutral solutions were taken to know the effect of the acidic medium. Magnetic field intensity, available in the laboratory and light wavelength, available in the laboratory. The range of possible values for each of these operating variables is presented in Table 4

Table 4 Range of Values of the Used Operating Variables

Parameters	**No. Variables**	**Values**
Feedstock	1	PO_4
Temperature, °C	1	Room temperature (19-22) °C
Initial concentration of PO_4 (ppm)	4	3.6,5.6,7.6,10.6
Dose of adsorbent (mg)	5	20,40,60,80,100
pH	5	3,4,5,7,9
Magnetic field strength (mTesla)	4	300,400,500,600
Wavelength light	6	white, green, red, yellow, blue, sun light
Contact time (minute)	8	5,15,30,45,60,75,90,100

4. Results and Descussion

4.1 Adsorption Isotherm

There are multiple models available for the representation of adsorption data, with the Freundlich and Langmuir models being the most extensively employed. These two models have been utilized in the current study. The calculation samples for the constants of these two models for the three adsorbents are included in Table 5 and Table 6. The aforementioned tables indicate that the correlation coefficient R2 value for the Langmuir model surpasses that of the Freundlich model. This implies that the Langmuir model provides a more accurate fit to the experimental data. The calculated adsorption capacities for Al2O3/AG, Al2O3 NPs, and Fly Ash respectively have been determined. Visual representations of the data, in accordance with the Freundlich and Langmuir models, can be seen in Figure 11.A and Figure 11.B, respectively. [16] and [17]

Freundlich model $\text{Log}Q_e = \log k_F + 1/n \log C_e$ (1)

Langmuir models $$\frac{C_e}{Qe} = \frac{1}{k_L Q_m} + \frac{1}{Q_m} C_e \quad (2)$$

Where;

C_e is equilibrium concentration (mg/L),

K_L is the Langmuir constant,

Q_e is are the adsorbate capacity (mg/g),

Q_m is the maximum adsorption capacity (mg/g),

K_F , n is the Freundlich constant.

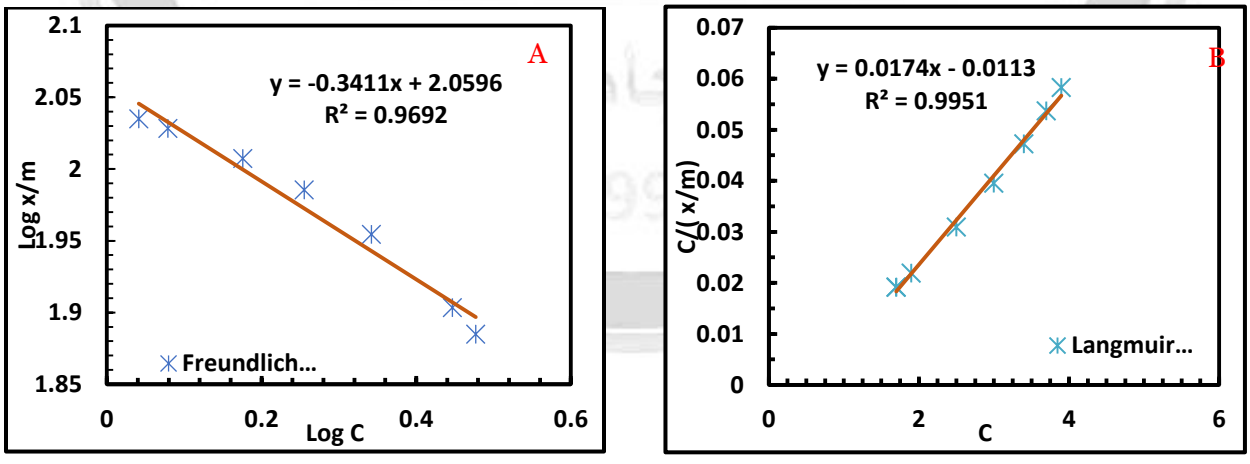

Figure 11 Adsorption Isotherm Parameters (C_i=7.6mg/L, Dose 60 mg, MF 500mT, pH 5, and Red Light, (A) Freundlich Linear Model (B) Langmuir Linear Model

Table 5 Freundlich and Langmuir Models Constants

Dose of Al_2O_3/ AG mg	Equilibrium concentration mg/L	Freundlich parameters			Langmuir parameters		
		n	k	R^2	a	b	R^2
Initial concentration of PO_4 = 7.6 mg/l, CT = 105 min, pH = 5, MFS =600 mT and Red Light							
20	1.311	-3.0367	114.6304	0.9531	-1.88889	196.0784	0.9824
40	1.258	-2.9788	172.901	0.9511	-2.20454	103.0927	0.9908
60	1.211	-2.9316	114.7097	0.9692	-2.11267	66.66666	0.9924
80	1.125	-2.9788	86.43706	0.9511	-2.10638	50.50505	0.9901
100	1.102	-2.79798	69.83931	0.9401	-2.02411	39.52569	0.9889

Table 6 Samples of Adsorption Constants Calculations

Initial concentration of PO_4 = 7.6 mg/l,Dose 60mg, CT = 105 min, pH = 5, MFS =600 mT and Red Light							
Adsorbent	**Equilibrium concentration mg/L**	**Freundlich constants**			**Langmuir constants**		
		n	k	R^2	a	b	R^2
Al_2O_3/ AG	1.211	-2.93169	114.7097	0.9692	-2.11267	66.66666	0.9924
Al_2O_3 NPs	2.654	-2.97885	172.901	0.9991	-2.20454	103.0927	0.9995
Fly Ash	2.845	-2.93169	114.7097	0.9959	-2.11267	66.66666	0.9971

4.1.1 Effect of Al_2O_3/AG Dose

Figure 12 shows the effect of AL_2O_3/AG dose on the adsorption capacity at pH of 5 and 9, respectively. The figure shows an increase in adsorption capacity when the dose of AL_2O_3/AG is increased. This trend agrees well with [18] and [19] . That higher initial concentration gives higher chance of collisions with adsorption sites. Moreover, the driving force of mass transfer is better, which will reduce the mass transfer resistance and increase the adsorption capacity[20]. The best dose for the adsorbent was 60 mg of AL_2O_3/AG which gave the best adsorption capacity.

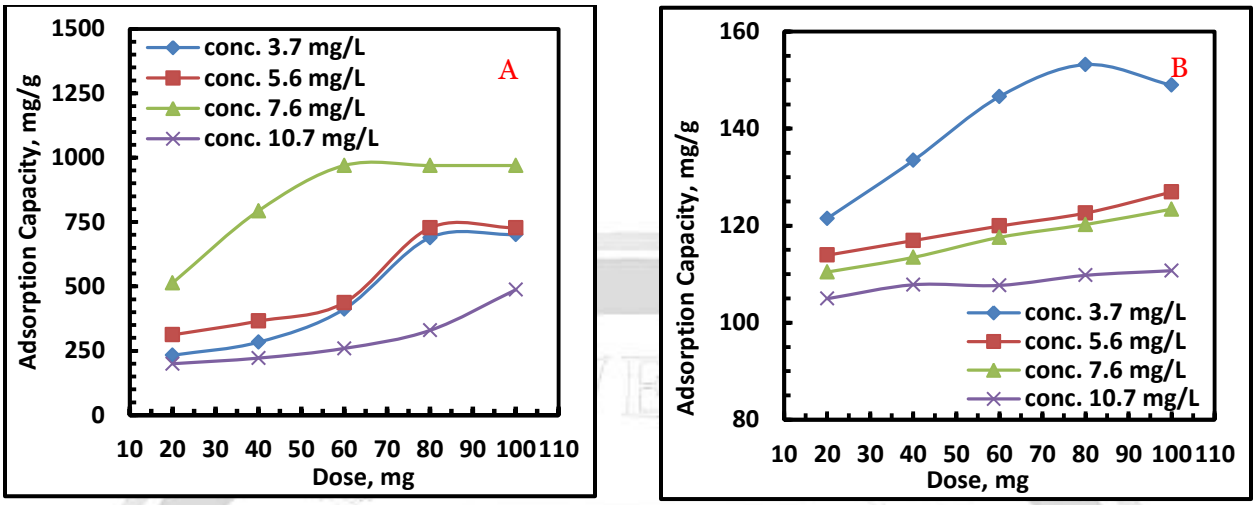

Figure 12 Effect of AL_2O_3/AG Dose on Adsorption Capacity, CT =100 Minute, and Red Light (A) pH =5, (B) pH =9.

4.1.2 Effect of Initial Concentration of Phosphate

Figure 13 shows decreasing effect of the initial concentration of phosphate on adsorption capacity for adsorbent AL_2O_3/AG dose at pH of 9 and 5, respectively. Here, it was noted that the increase in the initial concentration leads to a decrease in the adsorption capacity. Many researchers have stated that the more there is an increase in the initial concentration, the more possibility of meeting with adsorption sites of adsorbent or collision with those sites[21], [22] and [23]. The best adsorption capacity was at a concentration of 7.6 mg/L, and this concentration will be adopted when comparing the adsorbents.

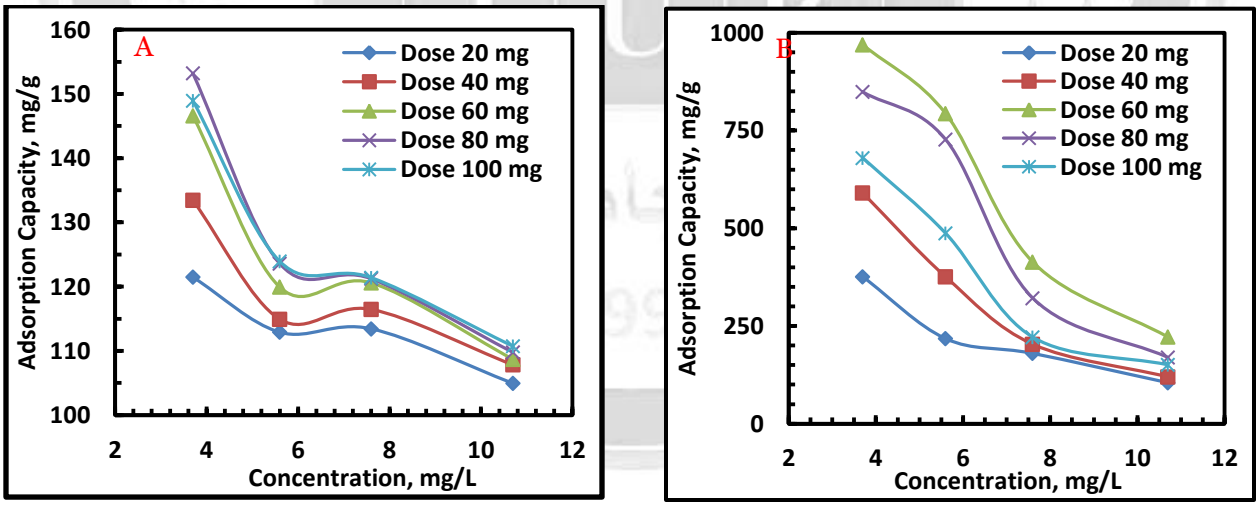

Figure 13 Effect of Initial Concentration of PO_4^{-3} on Adsorption Capacity for Adsorbent AL_2O_3/AG Dose at MF =500mT, CT =100 Minute, and Red Light, (A) pH =5, (B) pH =9.

ARTICLE
JOURNAL`S UNIVERSITY OF BABYLON FOR ENGINEERING SCIENCES (JUBES)
مـــجلـة جـــامعة بـــابـل للعلـــوم الهندسية
Vol. 32, No. 3. \ 2024 ISSN: 2616 - 9916

4.1.3 Effect of pH

Figure 14 explained the beginning by increasing the effect of the acid function pH on the adsorption capacity up to function 5. **Figure 14 A, B, Cand D** show a rapid rise of the pH function up to point 5 and then begin to gradually descend to the lowest point and then starting to gradually descend, this corresponds to[24]. When the pH is increased by more than 5, it will increase the competition between the hydrogen ion and the secondary ions, which leads to a decrease in the adsorption capacity and this consequently affects the adsorption sites [25].

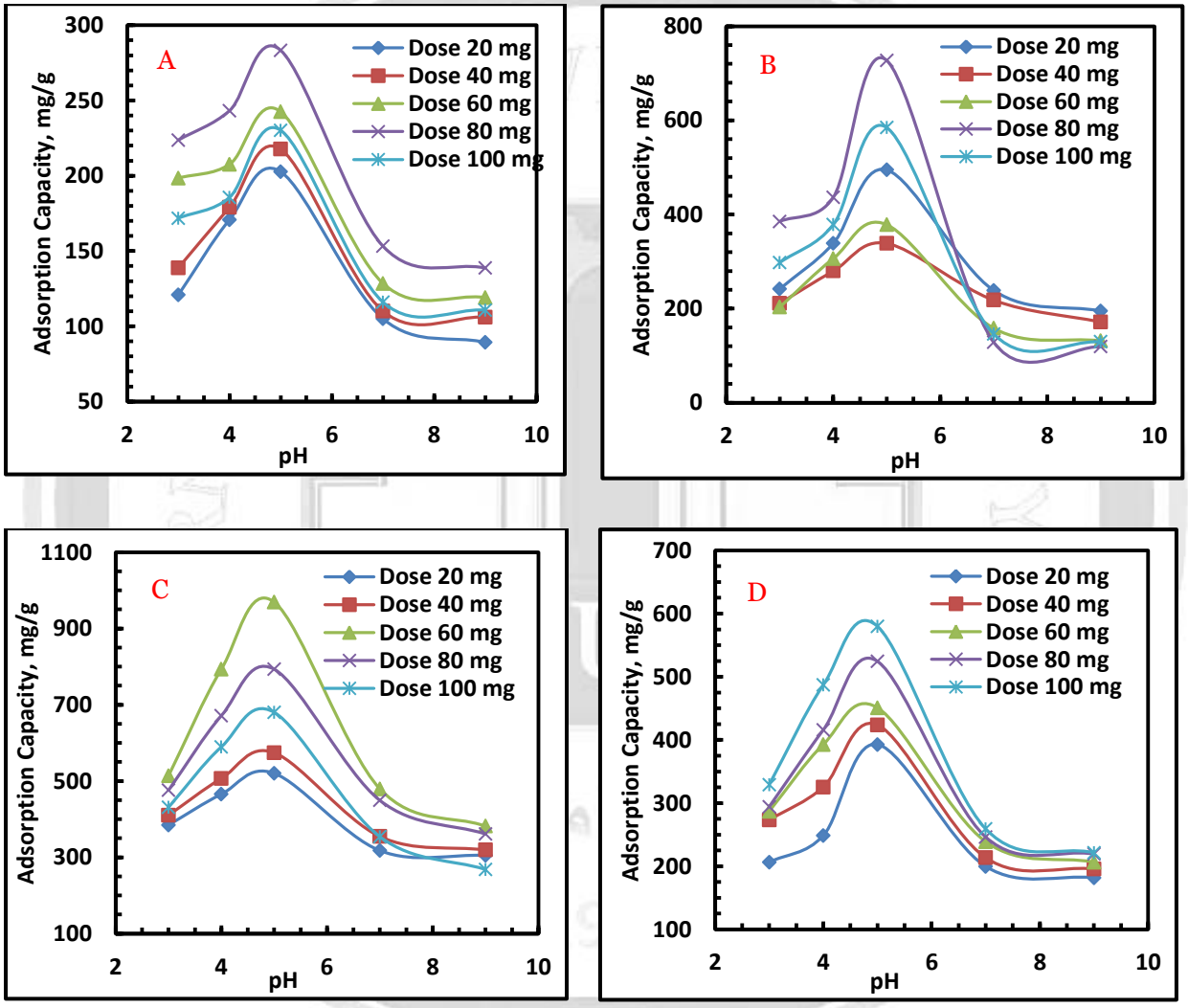

Figure 14 Effect of pH on Adsorption Capacity for Adsorbent AL_2O_3/AG Dose at MF 500mT, CT=100 Minute, and Red Light, (A) C_i =3.7 mg/L, (B) C_i =5.7 mg/L, (C) C_i =7.6 mg/L, (D) C_i =10.7 mg/L

4.1.4 Effect of Wavelength Light

It became clear the slow effect of light by exposing the sample to a different wavelength light intensity, where it begins to rise to stability at a time of 7 hours, and that the effect of the red color was higher than the rest **Figure 15.** As a result of the photocatalyst of some nanocomposites and the fact that the narrow wavelength of the red color has given the highest adsorption capacity for the rest of the colors, where the photoactivation is of great importance in stimulating the adsorption sites of the adsorbent to receive the largest amount of pollutants [26] and [27] .

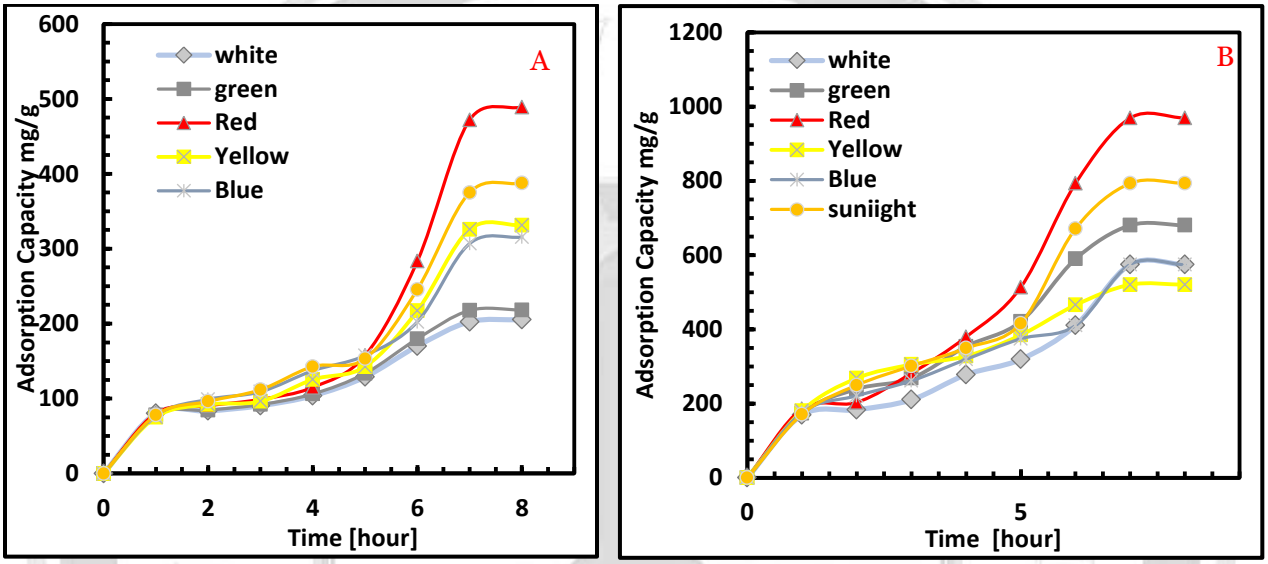

Figure 15 Effect of Contact Time on Adsorption Capacity at MFS =500 mTesla, and pH =5, (A) C_i= 3.7 mg/L, AL_2O_3/AG Dose of 80 mg, (B) C_i= 7.6 mg/L, AL_2O_3/AG Dose of 60 mg.

4.2 Adsorption Kinetics of Al_2O_3/AG

The purpose of this study was to analyze and assess the tendency of the process towards various kinetic models. During the investigation, it was noted that the observed process adhered strictly to the principles of pseudo-second-order kinetics. The pseudo-first-order equation

$$\log(q_e - q_t) = \log q_e - k1t \quad (3)$$

Where;

k_1 is the rate constants of the pseudo-first-order model equations, (min $^{-1}$),

q_e is the total of adsorbed material at equilibrium (mg. g $^{-1}$),

q_t is the total of adsorbed at time t (mg. g $^{-1}$),

t is irradiation time (hour) [28]

First, it was tested pseudo-first order equation and was determined by analyzing plots of the natural logarithm of the initial concentration divided by the concentration at a given time

against the duration of irradiation. **Figure 16.A** illustrates the linear correlation between the natural logarithm of the initial concentration divided by the concentration at a given time ($\ln(C_0/C_t)$) and the duration of irradiation; k1 and qe can be calculated from the slope and intercept.

Then it was tested pseudo-second-order kinetics from equation (4)

$$\frac{t}{q_t} = \frac{1}{k2{q_e}^2} + \frac{1}{q_e}t \qquad (4)$$

Where;

k_2 is the rate constant of the pseudo-second- order kinetic model equations, ($g.mg^{-1}.min^{-1}$) **Figure 16. B,** by the plot, is a straight line with a slope of 1/qe and intercept $1/(k2q_e^2)$. The calculated values of k2, qe and their corresponding correlation coefficient (R^2) are presented in **Table 7.** It shows the correlation coefficient (R^2) of the pseudo-second-order kinetic equation is more (>0.99). Therefore, the pseudo-second-order kinetic model can better describe Phosphate adsorption[29]. By determining the rate constant (k2) value, it was observed that the maximum value of k2 was 4.95×10^{-4} for red light. Similarly, the maximum of (R^2) values was 0.9996 for red light. In both instances, it was observed that the rate constant value was higher when photocatalysis was induced by red light in conjunction with adsorption. Hence, the findings validate that the physical composition of Al_2O_3/AG nanocomposites substantially enhances the photocatalytic activity compared to its pure nanoparticle counterparts when subjected to various light irradiation conditions. This is very consistent with [30], but it varies greatly with [31]

Table 7 Parameters of Phosphate Adsorption onto Al_2O_3/AG under Different Wavelength using Pseudo-First Order and Pseudo-Second-Order Kinetic Models.

Wave-lenght Light	C_0 ($mg.L^{-1}$)	q_e ($mg.g^{-1}$)	pseudo-first order equation			pseudo-second-order equation		
			K_1 (min^{-1})	q_e ($mg.g^{-1}$)	R^2	K_2 ($mg.g^{-1}.min^{-1}$)	q_e ($mg.g^{-1}$)	R^2
Red	7.6	108.333	2.50×10^{-3}	101.211	0.9942	4.95×10^{-4}	117.64	0.9996
Yellow	7.6	76.25	1.61×10^{-3}	71.367	0.9155	4.20×10^{-4}	80.63	0.9992
Green	7.6	107.5	2.47×10^{-3}	100.458	0.9862	1.33×10^{-4}	112.41	0.9979
Blue	7.6	62	1.85×10^{-3}	59.457	0.9821	3.95×10^{-4}	66.225	0.9983
White	7.6	103.333	2.40×10^{-3}	101.147	0.9886	1.61×10^{-4}	113.63	0.9936
Sunlight	7.6	64	2.35×10^{-3}	61.336	0.9586	3.31×10^{-4}	69.444	0.9975

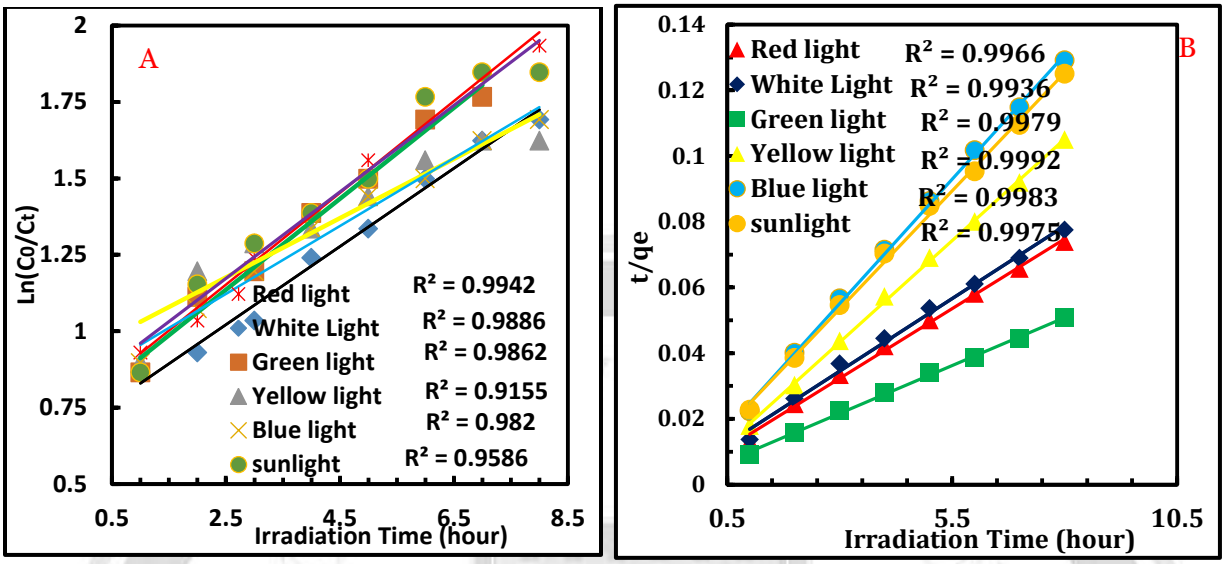

Figure 16 The Kinetic Model of Phosphate Ions Removal at C_i= 7.6 mg/L, AL_2O_3/AG Dose of 60 mg, MFS 600 mTesla,CT 8 hour, and pH= 5 (A) The Pseudo-First-Order Reaction, (B) The Pseudo-Second-Order Reaction

4.3. Comparison Among Al_2O_3/AG, Al_2O_3 NPs and Fly ash

Many experiments are conducted using Al_2O_3 NPs and fly ash adsorbents based on the best results of the previous schemes. The obtained results are compared with those using Al_2O_3/AG.

Figures 17, 18, 19, and **20** show the effect of dose, pH, magnetic field strength, and wave length respectively on phosphate removal efficiency for the three adsorbents. It is clear that Al_2O_3/AG gives the highest removal followed by Al_2O_3 NPs and fly ash. Although Al_2O_3/AG does not have smaller particle size, it has the higher surface area according to BET analysis **Table 3** it gives the highest removal. The reason for this behavior is to the physical composition of Al_2O_3/AG nanocomposites most attractive to phosphate and its higher surface area which provides more adsorption sites[32]. That adsorption process depends on the nature and properties of adsorbent and adsorbate. Adsorbent properties include surface area which is increased with the decrease of particle size[33].

That many parameters affecting the adsorption process which are the basis of a lot of research to find the optimum conditions for adsorption process[34]and [35]. These parameters include initial pollutant concentration, pH, adsorbent dosage, and particle size abbreviated in **Table 8**. A lot of work proved that the adsorption is increased with the increase of the adsorbent surface are [36] and [37].

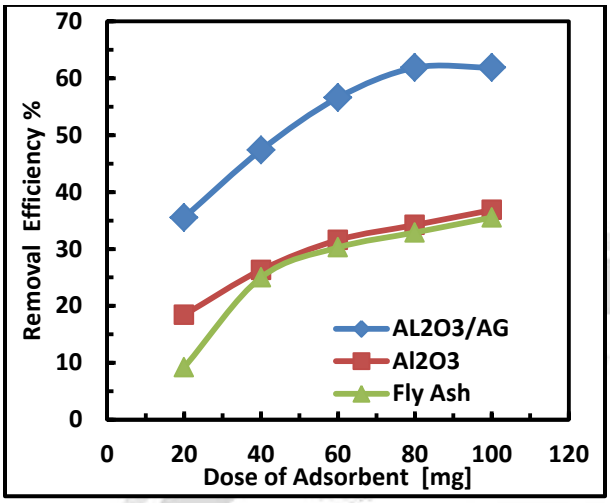

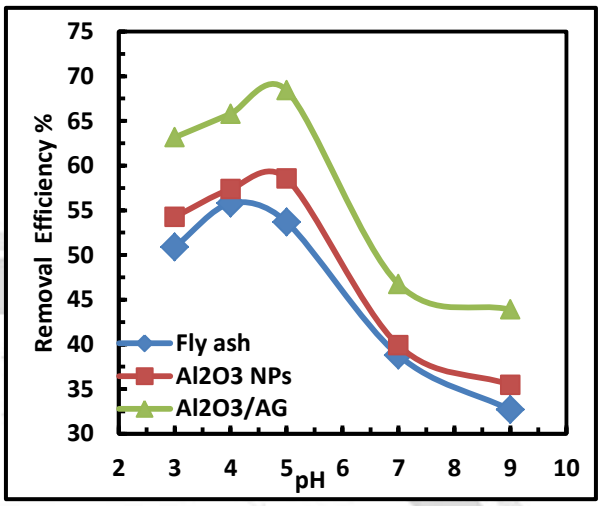

Figure 17 Effect of Different Adsorbent Dose on Removal Efficiency of PO_4^{-3}

Figure 18 Effect of pH on Removal Efficiency

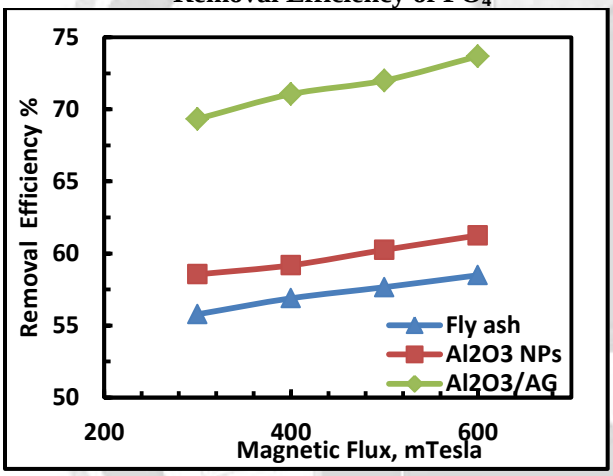

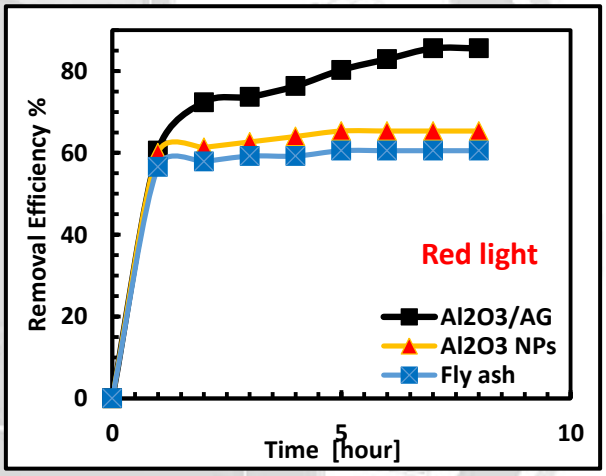

Figure 19 Effect of Magnetic Flux Strength on Removal Efficiency

Figure 20 Effect of Contact Time on Removal Efficiency

Table 8 Summary of the Comparison (Al_2O_3 NPs, Fly Ash and Al_2O_3/AG Nanocomposites) for the Adsorption Phosphate.

Parameters	Al_2O_3/AG	Al_2O_3 NPs	Fly ash
SEM images, particle size range, (nm)	43.24 - 97.71	50	31.66-53.64
Surface Area, (m^2/g)	124.25	51.235	46.438
Optimumadsorbent dose, (mg)	60	80	100
Optimum pH	5	5	4
Optimum Magnetic Flux Strength, (mTesla)	500	500	500
Optimum Wave length Light	red	red	Sun light
Adsorption isotherm models	Langmuir	Langmuir	Langmuir
R^2	0.9924	0.9995	0.9971
Adsorption capacity, (mg/g)	63.24 - 969.38	59.79 - 244.68	54.11 - 219.02
Highest removal efficiency, (%)	85.52	65.33	63.15

5. Conclusions

- The synthesized Al_2O_3/AG nanocomposites is better than Al_2O_3 NPs and fly ash in phosphate removal.
- pH at 5 is the best effective parameter of the phosphate removal process for all Al_2O_3/AG and Al_2O_3 NPs, but pH 3 is the best effective for fly ash in phosphate removal.
- The effect of the magnetic field and wavelength is not quickly and requires time in addition to being ineffective at low concentrations.
- The best dose for Al_2O_3/AG nanocomposites was 60 mg/L and the best initial concentration of phosphate was 7.6 mg/L.

1. The increase in dose is directly proportional to the adsorption capacity while the initial concentration is inversely proportional to the adsorption capacity.

- The maximum removal efficiency is (85.52%) for Al_2O_3/AG nanocomposites and the lowest removal efficiency is (2.88 %) for fly ash.
- It was shown that changing the pH is very effective in increasing the phosphate removal rate, as the acidic medium is more effective in removing phosphates.
- The effect of light does not appear during the first hour, but for up to about 7 hours, and it has little effect, but it must be taken into account, and the red color appears more effective than others in removing phosphates.
- It is found that the Langmuir model fit the adsorption capacity while the pseudo-second-order kinetic model is fit the adsorption.
- The surface area of AL_2O_3/AG nanocomposites was 124.255 $m^2 . g^{-1}$, AL_2O_3 NPs was 51.235 $m^2 . g^{-1}$, and fly ash was 46.438 $m^2 . g^{-1}$.

Nomenclature

Abbreviations:	**Description**
AG	Aloe vera Gum
a, b	Constants of Langmuir.
ATP	Adenosine triphosphate
C_o	Concentration
C_e	Equilibrium concentration
C_f	Final concentration
C_i	Initial concentration
COD	Chemical oxygen demand
CT	Contact Time
DNA	Deoxyribonucleic acid
K	Freundlich's constant
MO	Metal oxide
MOFs	Metal-organic frameworks
NPs	Nanoparticals
pH	Indicates how acidic or basic a substance is, and the scale ranges from 0 to 14
ppm	parts per million

R%	Removal efficiency
R^2	Correlation coefficient
RNA	Ribonucleic acid
TSP	Trisodium phosphate with the chemical formula Na_3PO_4
VFAs	Volatile fatty acids
WWTPs	Wastewater treatment plants
XRD	X-ray diffractometers

References

[1] J. Serna and C. Bergwitz, "Importance of dietary phosphorus for bone metabolism and healthy aging," *Nutrients*, vol. 12, no. 10, p. 3001, 2020.

[2] S. Wagner, T. Hüffer, P. Klöckner, M. Wehrhahn, T. Hofmann, and T. Reemtsma, "Tire wear particles in the aquatic environment-a review on generation, analysis, occurrence, fate and effects," *Water Res.*, vol. 139, pp. 83–100, 2018.

[3] T. J. Smayda, "Complexity in the eutrophication–harmful algal bloom relationship, with comment on the importance of grazing," *Harmful Algae*, vol. 8, no. 1, pp. 140–151, 2008.

[4] Z. Yin *et al.*, "A new approach to removing and recovering phosphorus from livestock wastewater using dolomite," *Chemosphere*, vol. 255, p. 127005, 2020.

[5] A. Asfaram, M. Ghaedi, S. Agarwal, I. Tyagi, and V. K. Gupta, "Removal of basic dye Auramine-O by ZnS: Cu nanoparticles loaded on activated carbon: optimization of parameters using response surface methodology with central composite design," *RSC Adv.*, vol. 5, no. 24, pp. 18438–18450, 2015.

[6] H. Dong, M. German, L. Tian, and A. K. SenGupta, "Multifunctional ion exchange pretreatment driven by carbon dioxide for enhancing reverse osmosis recovery during impaired water reuse," *Desalination*, vol. 485, p. 114459, 2020.

[7] H. M. Azam *et al.*, "Phosphorous in the environment: characteristics with distribution and effects, removal mechanisms, treatment technologies, and factors affecting recovery as minerals in natural and engineered systems," *Environ. Sci. Pollut. Res.*, vol. 26, pp. 20183–20207, 2019.

[8] J. Y. Lee *et al.*, "Nutrient removal from hydroponic wastewater by a microbial consortium and a culture of Paracercomonas saepenatans," *N. Biotechnol.*, vol. 41, pp. 15–24, 2018.

[9] D. Pathania, R. Katwal, G. Sharma, M. Naushad, M. R. Khan, and H. Ala'a, "Novel guar gum/Al2O3 nanocomposite as an effective photocatalyst for the degradation of malachite green dye," *Int. J. Biol. Macromol.*, vol. 87, pp. 366–374, 2016.

[10] H. Hassena, "Photocatalytic degradation of methylene blue by using Al2O3/Fe2O3 nano composite under visible light," *Mod. Chem. Appl.*, 2016.

[11] M. Velu *et al.*, "Fabrication of nanocomposites mediated from aluminium nanoparticles/Moringa oleifera gum activated carbon for effective photocatalytic removal of nitrate and phosphate in aqueous solution," *J. Clean. Prod.*, vol. 281, p. 124553, 2021.

[12] K. Motevalli, M. Ebadi, and Z. Salehi, "Synthesis of Ag–AgO/Al 2 O 3 nanocomposite via a facile two-step method for photodegradation of methylene blue," *J. Mater. Sci. Mater. Electron.*, vol. 28, pp. 13024–13031, 2017.

[13] Z. Bao, L. Ye, B. Fang, and L. Zhao, "Synthesis of Fe 0.32 Co 0.68/γ-Al 2 O 3@ C nanocomposite for depth treatment of dye sewage based on adsorption and advanced catalytic oxidation," *J. Mater. Chem. A*, vol. 5, no. 14, pp. 6664–6676, 2017.

[14] S.-W. Yu and H.-J. Choi, "Application of hybrid bead, persimmon leaf and chitosan for the treatment of aqueous solution contaminated with toxic heavy metal ions," *Water Sci. Technol.*, vol. 78, no. 4, pp. 837–847, 2018.

[15] S. Daneshgar, A. Callegari, A. G. Capodaglio, and D. Vaccari, "The potential phosphorus crisis: resource conservation and possible escape technologies: a review," *Resources*, vol. 7, no. 2, p. 37, 2018.

[16] A. B. Albadarin, C. Mangwandi, H. Ala'a, G. M. Walker, S. J. Allen, and M. N. M. Ahmad, "Kinetic and thermodynamics of chromium ions adsorption onto low-cost dolomite adsorbent," *Chem. Eng. J.*, vol. 179, pp. 193–202, 2012.

[17] D. Itrogiannis *et al.*, "Removal of phosphate from aqueous solutions by adsorption onto Ca (OH) 2 treated natural clinoptilolite," *Chem. Eng. J.*, vol. 320, pp. 510–522, 2017.

[18] M. H. Salmani, M. Abedi, S. A. Mozaffari, and H. A. Sadeghian, "Modification of pomegranate waste with iron ions a green composite for removal of Pb from aqueous solution: equilibrium, thermodynamic and kinetic studies," *AMB Express*, vol. 7, no. 1, pp. 1–8, 2017.

[19] J. Di *et al.*, "Adsorption behaviors and mechanisms of Cu2+, Zn2+ and Pb2+ by magnetically modified lignite," *Sci. Rep.*, vol. 12, no. 1, p. 1394, 2022.

[20] G. T. Tee, X. Y. Gok, and W. F. Yong, "Adsorption of pollutants in wastewater via biosorbents, nanoparticles and magnetic biosorbents: A review," *Environ. Res.*, vol. 212, p. 113248, 2022.

[21] M. M. Ibrahim and I. A. Jaddo, "Removal of some hydrocarbon pollutants from Baiji oil refinery wastewater using granular activated carbon column," *Tikrit J. Eng. Sci.*, vol. 21, no. 3, pp. 84–95, 2014.

[22] R. Farouq, "Coupling adsorption-photocatalytic degradation of methylene blue and maxilon red," *J. Fluoresc.*, vol. 32, no. 4, pp. 1381–1388, 2022.

[23] T. K. Sen, "Adsorptive Removal of Dye (Methylene Blue) Organic Pollutant from Water by Pine Tree Leaf Biomass Adsorbent," *Processes*, vol. 11, no. 7, p. 1877, 2023.

[24] A. T. Adeolu, O. T. Okareh, and A. O. Dada, "Adsorption of chromium ion from industrial effluent using activated carbon derived from plantain (Musa paradisiaca) wastes," *Am J Env. Prot [Internet]*, vol. 4, no. 1, pp. 7–20, 2016.

[25] A. Subratti, J. L. Vidal, L. J. Lalgee, F. M. Kerton, and N. K. Jalsa, "Preparation and characterization of biochar derived from the fruit seed of Cedrela odorata L and evaluation of its adsorption capacity with methylene blue," *Sustain. Chem. Pharm.*, vol. 21, p. 100421, 2021.

[26] M. Romero Saez *et al.*, "Notable photocatalytic activity of TiO2-polyethylene nanocomposites for visible light degradation of organic pollutants," 2017.

[27] A. Diacon *et al.*, "New carbon/ZnO/Li2O nanocomposites with enhanced photocatalytic activity," *Sci. Rep.*, vol. 9, no. 1, p. 16840, 2019.

[28] X. Guo and J. Wang, "A general kinetic model for adsorption: theoretical analysis and modeling," *J. Mol. Liq.*, vol. 288, p. 111100, 2019.

[29] F. H. Yahya, "using of magnetic nanoparticles to remove Cu +2 from aqueous solution," 2022.

[30] J. Wang, X. Tong, and S. Wang, "Zirconium-modified activated sludge as a low-cost adsorbent for phosphate removal in aqueous solution," *Water, Air, Soil Pollut.*, vol. 229, pp. 1–10, 2018.

[31] S. Shajahan, P. Arumugam, R. Rajendran, and A. P. Munusamy, "Optimization and detailed stability study on Pb doped ceria nanocubes for enhanced photodegradation of several anionic and cationic organic pollutants," *Arab. J. Chem.*, vol. 13, no. 1, pp. 1309–1322, 2020.

[32] M. M. I. Aldoury, N. N. Ismaeal, and M. J. Mahdi, "Softening of Groundwater at Samarra City by Electromagnetic Polarization," in *IOP Conference Series: Earth and Environmental Science*, IOP Publishing, 2022, p. 12009.

[33] B. Tamamushi, "Factors influencing the adsorption from solutions," *Adsorpt. from Solut.*, pp. 79–86, 1983.

[34] J. S. Baker and S. J. Judd, "Magnetic amelioration of scale formation," *Water Res.*, vol. 30, no. 2, pp. 247–260, 1996.

[35] E. Rápó and S. Tonk, "Factors affecting synthetic dye adsorption; desorption studies: a review of results from the last five years (2017–2021)," *Molecules*, vol. 26, no. 17, p. 5419, 2021.

[36] B. M. Fahad, N. S. Ali, and T. T. Hameed, "The Influence of Eggshell Particle Sizes on the Adsorption of Organic Dye," *Iraqi J. Chem. Pet. Eng.*, vol. 18, no. 1, pp. 111–120, 2017.

[37] E. H. Gora, S. G. Saldana, L. M. Casper, V. Coll Sijercic, O. A. Giza, and R. L. Sanders, "Effect of Exhausted Coffee Ground Particle Size on Metal Ion Adsorption Rates and Capacities," *ACS omega*, vol. 7, no. 43, pp. 38600–38612, 2022.

ARTICLE

JOURNAL`S UNIVERSITY OF BABYLON FOR ENGINEERING SCIENCES (JUBES)

مـــجلـة جـــامعة بـــابـل للعلـــوم الهندسية

Vol. 32, No. 3. \ 2024 ISSN: 2616 - 9916

مقارنه بين ثلاث مواد مازة وهي المركبات النانوية Al_2O_3/ محملة على جل نبات الصبار، الالومينا النانوية Al_2O_3 والرماد المتطاير في إزالة الفوسفات من نهر دجلة

غالب جاسم كاظم الصميدعي[1] مزهر مهدي أبراهيم الدوري[2]

1قسم الهندسة الكيميائية، كلية الهندسة، جامعة تكريت، تكريت، العراق

Email: Kalab.j.kadem44336@st.tu.edu.iq, ORCID: https://orcid.org/0009-0006-5429-8852

2قسم هندسة النفط وتكرير الغاز، كلية هندسة العمليات النفطية، جامعة تكريت، تكريت، العراق

Email: samuzhermahdi@tu.edu.iq ; ORCID: https:// orcid.org/0000-0002-5149-945X

الخلاصة

تم استخدام مواد نانوية حديثة وواعدة وصديقة للبيئة كمواد ماصة، [الجسيمات النانوية AL_2O_3/ المحمل على صمغ الصبار]. وهي مادة تفرز بصورة طبيعية من (Aloe vera plant) لانتاج جسيمات نانوية باستخدام طريقة سول جل لزيادة مساحة السطح لإزالة الفوسفات إضافة الى الجسيمات النانوية AL_2O_3 والرماد المتطاير.

ظروف التشغيل المستخدمه في هذه الدراسة هي الجرع للجسيمات النانوية (AL_2O_3 / AG) (20–100 ملغم) ، تركيز الأيونات الابتدائي 3.7–10.7 (C_i) ملغم / لتر. درجة الحموضة 3–9، وقت التلامس 5–100 (CT) دقيقة، شدة المجال المغناطيسي 300–500 mTesla (MF)، والطول الموجي للضوء (الأبيض والأخضر والأحمر والأصفر والأزرق وضوء الشمس). أجريت تجارب دفعية باستخدام جهاز هانا عالي المدى لقياس تركيز الفوسفات.

أشارت النتائج إلى أن الرقم الهيدروجيني 5، 100 CT دقيقة، الجرعة 60 ملغ، الضوء الأحمر، و Ci من PO_4^{-3} عند 7.6 ملغم / لتر. وجد أن نموذج امتزاز Langmuir يناسب إلى حد ما البيانات التجريبية. في حين أن النموذج الحركي الزائف من الدرجة الثانية يناسب الامتزاز. تزداد قدرة الامتزاز مع انخفاض التركيز الأولي للملوث (الفوسفات) وتتناسب طرديا مع جرعة الممتزات النانوية AL_2O_3 / AG.

تمت مقارنة أفضل الظروف التي تم الحصول عليها باستخدام AL_2O_3 / AG مع الرماد المتطاير و AL_2O_3 NPs. تم قياس مساحة سطح المركبات النانوية AL_2O_3 / AG حيث كانت 124.255 م^2. غم$^{-1}$. تم استخدام أفضل الظروف التشغيلية والتي أعطت أعلى نسبة إزالة لاختبار كل من AL_2O_3 NPs والرماد المتطاير. وقد تم اثبات أن AL_2O_3 / AG يعطي إزالة أعلى من AL_2O_3 NPs والرماد المتطاير.

الكلمات الدالة: *سعة الامتزاز، هلام الالوفيرا، الجسيمات النانوية للألومينا، شدة الضوء، الفوسفات.*